24th INTERNATIONAL CONGRESS ON SOUND AND VIBRATION
23–27 July 2017, London

ON THE CHOICE OF CONDENSATION FUNCTIONS FOR MID-TO-HIGH FREQUENCY VIBROACOUSTIC MODELLING

Zhongyu Hu and Li Cheng

The Hong Kong Polytechnic University, Department of Mechanical Engineering, Hung Hom, Kowloon, Hong Kong, China
email: zhongyu.hu@connect.polyu.hk

Laurent Maxit

INSA Lyon, Laboratoire Vibrations Acoustique, 25 bis, avenue Jean Capelle, 69621 Villeurbanne Cedex, FRANCE

The analysis of vibro-acoustic systems in the mid-to-high frequency range is computational costly and technically challenging. Sub-structuring methods are often employed in such cases, which allow reducing the number of degrees of freedoms at the interface between sub-systems. In the same category, the Condensed Transfer Function (CTF) approach has previously been proposed, to be improved and further explored in this paper. In the CTF approach, the uncoupled sub-systems are first modelled separately, by approximating the force and the velocity distribution over the coupling surface by a set of so-called condensation functions. By applying the force equilibrium and velocity continuity conditions, the overall system can be assembled and solved accordingly. In this paper, a panel-cavity system is modelled with the CTF approach, in a wide frequency band which covers the critical frequency of the panel and embraces a relatively high modal density. It is demonstrated that the calculation efficiency of the CTF method can be greatly increased by properly selecting the condensation functions and exploring their physical characters. As a result, the previously established convergence rule based on the gate functions can be relaxed. More specifically, the condensation functions such as exponential functions exhibit strong physical features. For a given frequency band, the condensation functions that match the structural wavelength properties dominate the system response. Therefore, the velocity and energy distribution on the coupling surface can be described by only a subset of the CTFs involving only a few terms. This leads to a significant reduction of the matrix size to be solved and consequently an increased computational efficiency.
Keywords: vibro-acoustic, sub-structuring method, mid-to-high frequency

1. Introduction

The development of dedicated methods for the mid-to-high frequency vibro-acoustic modelling has always been a challenge and arousing vast interest in the vibro-acoustic community. Methods based on sub-structuring philosophy are often employed in such cases. Upon proper handling of the interfaces between sub-systems, these methods allow reducing the number of degrees of freedoms involved in the calculation. Among existing methods, the Patch Transfer Functions (PTF) method is a representative example[1]. The PTF method allows the subsystems to be modelled separately, before being assembled along the coupling surface based on continuity conditions. The coupling surface can be either the interface between a structure domain and an acoustic domain[2], or between two acoustic domains[1]. The method consists in dividing the coupling surface into patches using a criterion based on the wavelength of the propagative waves on the coupling surface. Then, for each uncoupled subsystem, the transfer functions between each pair of patches should be calculated. In the

final stage, the patch transfer functions are assembled to predict the behaviour of the global system. The method has been applied to airborne noise predictions[3], sound transmission in buildings[4], and transmission loss predictions in silencer designs[5] etc.. The method was extended and cast into a more general form, referred to as Condensed Transfer Function (CTF) approach[6]. The CTF approach extends the patches to any orthogonal function sets along the coupling surface such as the complex exponential functions and the Chebyshev polynomials, referred to as Condensation Functions (CF). This method has been applied to the modelling of non-axisymmetric internal frames for the investigation of the radiation efficiency and energy distributions [7]. However, the research on CTF approach, has only focused on the cases of line coupling like frame-shell connections. This paper examines the use of different types of condensation functions to the problem of structure-acoustic coupling over a surface. The choice of different types of CFs as well as their impact on the modelling efficiency and accuracy will be the focus of the paper. In particular, we will focus on the use of complex exponentials as condensation functions. The basic principle of the CTF approach will be firstly presented using a benchmark problem of a plate-cavity system, including the system model and the convergence rule. The performance of the gate functions (patch functions) and exponential functions will be compared afterwards and the advantage of exponential functions will be demonstrated.

2. Theoretical Analyses

In this section, the basic principle of the CTF method is applied to model a plate-cavity system. Additionally, examples of condensation functions as well as the rule to warrant their convergence are given.

2.1 Basic theory of the CTF method

Consider a rectangular acoustic cavity with one of its walls covered by a vibrating plate and the others being acoustically rigid, as shown in Fig.1. The plate, simply supported along all four edges, is subjected to a prescribed sound pressure excitation P^e. The two structural (panel) and acoustic (cavity) subsystems are coupled along their interface Ω and will be denoted by superscript *s* and *a*, respectively.

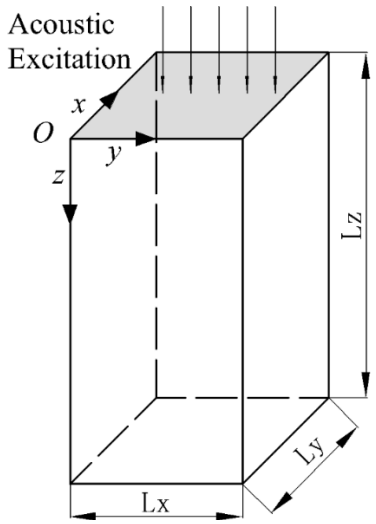

Fig. 1: The cavity-panel configuration and coordinate system.

A set of N orthonormal functions $\{\varphi_i\}_{1\leq i\leq N}$ is employed to approximate the velocities and the forces on the coupling interface, which will be referred to as condensation functions (CF) in this paper. Notice that the coupling interface is two dimensional. For each subsystem α, the condensed mobility, also referred to as the CTF between $\varphi_{ij}(x,y) = \varphi_i(x)\varphi_j(y)$ and $\varphi_{kl}(x,y) = \varphi_k(x)\varphi_l(y)$, is defined by applying an excitation pressure $P^\alpha(x,y) = \varphi_i(x)\varphi_j(y)$ on Ω as:

$$Y_{kl,ij}^{\alpha} = \frac{<\overline{U}_{ij}^{\alpha}, \varphi_{kl}>}{<P^{\alpha}, \varphi_{ij}>} = <\overline{U}_{ij}^{\alpha}, \varphi_{kl}>, \tag{1}$$

in which $<f, g>$ is a scalar product defined as $\int_{\Omega} f(x,y)g^*(x,y)dS$ with g^* being the complex conjugate of g, and $\overline{U}_{ij}^{\alpha}$ is the uncoupled velocity on Ω when subsystem α is subjected to the excitation $P^{\alpha}(x,y) = \varphi_i(x)\varphi_j(y)$. Additionally, the uncoupled condensed velocity $\tilde{u}_{ij}$ of the subsystem α is defined by

$$\tilde{u}_{ij}^{\alpha} = <\tilde{U}^{\alpha}, \varphi_{ij}>, \tag{2}$$

where $\tilde{U}^{\alpha}$ is the uncoupled velocity of the subsystem α at Ω when only external excitation exists. Then one obtains the approximations of the uncoupled velocities and forces for each subsystem as

$$\begin{cases} \tilde{U}^s(x,y) \simeq \sum_i \sum_j \tilde{u}_{ij}^s \varphi_i(x)\varphi_j(y) \\ \tilde{U}^a(x,y) \simeq \sum_i \sum_j \tilde{u}_{ij}^a \varphi_i(x)\varphi_j(y) \end{cases}, \text{ and } \begin{cases} \tilde{P}^s(x,y) \simeq \sum_i \sum_j \tilde{p}_{ij}^s \varphi_i(x)\varphi_j(y) \\ \tilde{P}^a(x,y) \simeq \sum_i \sum_j \tilde{p}_{ij}^a \varphi_i(x)\varphi_j(y) \end{cases}, \tag{3}$$

where u_{ij}^{α} and f_{ij}^{α} are the amplitudes of uncoupled velocity and external excitation of subsystem α with respect to condensation function φ_{ij}. In the present case, $\tilde{p}^a = 0$ and $\tilde{p}^s = P^e$. For the present linear system, the velocity and force on the coupling interface can be calculated following the superposition principle, given by:

$$\begin{cases} u_{ij}^s = \tilde{u}_{ij}^s + \sum_{i,j} Y_{ij,kl}^s p_{kl}^s \\ u_{ij}^a = \sum_{i,j} Y_{ij,kl}^a p_{kl}^a \end{cases}. \tag{4}$$

On the other hand, the velocity continuity and force equilibrium principle along the coupling interface yield

$$\begin{cases} U^s = U^a = U^c \\ P^s = -P^a = P^c \end{cases}. \tag{5}$$

in which the superscript *c* represents variables of the coupled system at the coupling interface. According to the orthogonal property of the condensation functions, Eq. (6) gives the variables relationship deduced from Eq. (5):

$$\begin{cases} u_{ij}^s = u_{ij}^a \\ p_{ij}^s = -p_{ij}^a \end{cases}. \tag{6}$$

For the acoustic cavity, the condensed impedance matrix Z^a, which satisfies $Z^a = [Y^s]^{-1}$, is preferred rather than the condensed mobility. Substituting Eq. (6) and Z^a into Eq. (4), U^c can be finally calculated as:

$$U^c = \left[I + Y^s Z^a \right]^{-1} \tilde{u}. \tag{7}$$

2.2 Two examples of condensation functions and their convergence rules

2.2.1 Gate functions

The gate functions are defined as:

$$\varphi_i(x) = \begin{cases} \frac{1}{\sqrt{L_g}} & \text{if } (i-1)L_x \le x \le iL_x \\ 0 & \text{elsewhere} \end{cases}, \tag{17}$$

where L_g is the length of each gate function. Figure 2 explicitly shows the working principle of gate functions on the coupling interface, in which *i* and *j* are the gate indices for *x* and *y* directions, respectively. Each condensed mobility term $Y_{kl,ij}$ physically corresponds to the velocity response U_{kl} when

a unit excitation P_{ij} is applied, as illustrated in Fig. 2. In this case, the general CTF method retreats to the previous patch transfer function (PTF) method as a special case. Owing to the intuitive and explicit physical meaning of the gate functions, the corresponding condensed mobility and impedance can be obtained from various numerical calculations, or even from experimental measurements.

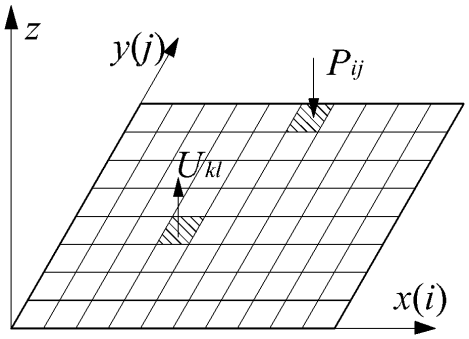

Fig. 2: The working principle of gate functions.

As to the convergence criterion, it is well accepted that at least two functions are needed to describe a wavelength. Therefore, for a given structural or acoustical wavelength λ, the length of the gate functions L_g should satisfy:

$$L_g \leq \frac{\lambda}{2}. \tag{18}$$

2.2.2 Exponential functions

The exponential functions are described by

$$\varphi_i(x) = \frac{1}{\sqrt{L_x}} \exp(j\frac{2i\pi x}{L_x}) \tag{19}$$

The functions form an orthonormal set with the defined scalar product for $i \in [0, \pm1, \pm2, \ldots, \pm N_{max}]$. Different from the case of the gate functions in which the coupling interface is divided into "patches", the working principle of the exponential functions spatially decompose the velocity and the force over the entire coupling interface.

The truncation criterion applied to the decomposition series is based on the same principle as that of the gate functions, written as:

$$N_{max} \geq \frac{2L_x}{\lambda} - 1. \tag{20}$$

3. Numerical validations and analyses

In the following numerical analyses, the dimension of the cavity is set to be 2.5m×2m×3m (x×y×z). The simply supported plate is 1.8mm thick, located at z=0. The Young's modules of the panel is 7.2×10^{10}Pa; the panel's Poisson's ratio is 0.2; the panel density is 2.53×10^{3}kg/m^3; η^a and η^p are set to 0.001 and 0.01 for the cavity and the plate, respectively. An oblique acoustic excitation with an amplitude of 1Pa is impinging on the plate, with both the dihedral angle and the intersection angle with x axis being 45°. The purpose of using oblique incident excitation is to excite more panel modes and get the complexity needed for analyses. The frequency band of interest is [0, 1000] Hz. Additionally, according to Eq. (18), the number of condensation functions should be determined by the shorter wavelength among the subsystems. Because the number used for the two subsystems should be equal so that they can be assembled together in Eq. (7), the function number will be selected following the subsystem whose wavelength at 1000Hz is shorter. In the present case, the shorter wavelength comes from the acoustic system with a smallest wavelength of 0.17m. This results in 174 condensation functions. In the present case, 180 gate functions will be used (15 for x direction and 12

for *y* direction) in the calculation. For exponential functions, N_{max} =6 is selected giving 169 terms in the calculation.

3.1 Pressure Validations

The sound pressure is calculated at a receiving point chosen at (0.5, 1.3, 2)m. The sound pressure level (SPL) results are given in Fig. 5, in which the CTF results using two different CFs are compared with the reference solution obtained from the reference results. The latter was calculated using modal method, which has been fully validated in a previous study. It can be seen that the pressure predictions by both types of CFs agree well with the reference result in the low frequency range. However, the performance of the gate functions slightly deteriorates as compared with the exponential functions in relatively high frequency range, especially at the troughs of the curves where system becomes less dynamic. Upon averaging the acoustic pressure within the entire cavity, the averaged overall SPL is shown in Fig. 6, leading to the same observation as that obtained in Fig. 5. Generally speaking, the truncation criteria allow acceptable calculation accuracy for both type of CFs, knowing however exponential functions perform better at non-resonance frequencies in both single point and overall predictions.

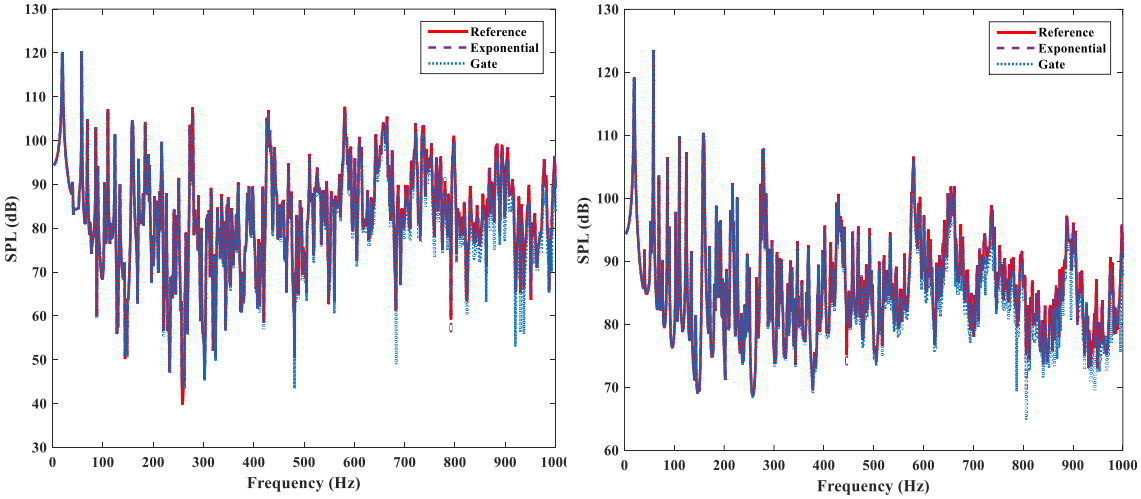

(a) (b)

Fig. 5: SPL with reference to 2x10^{-5}Pa: (a) at (0.5, 1.3, 2)m; (b) overall within the cavity.

3.2 Analyses of the condensed variables

Figures 5 and 6 imply that the accuracy of the model can be improved by properly choosing the condensation functions. Particularly, the exponential functions behave better than the gate functions in mid-to-high frequency range, which will be the main focus of discussions. In this section, we will analyze the three main variables, namely the condensed mobility, the condensed impedance, and the condensed velocity of the system, so as to reveal the underlying mechanisms of such phenomena. To this end, we define the mid frequency range as the frequency staring from which the modal overlap factor of either the panel or that of the cavity starts to be larger than one. In the present case, the frequency range begins from 593Hz. Therefore, the variable analyses will focus on the frequencies higher than this value.

3.2.1 Condensed impedance and mobility

Firstly for the cavity, the condensed impedance $Z^{a}_{kl,ij}$ of the exponential functions at 794 Hz, which is the central frequency of a one third octave frequency band, is shown in Fig. 7a. For gate functions, the *x*-axis and *y*-axis denote the serial number of condensation functions φ_{ij} following the order: [φ_{11}, φ_{12}, …φ_{1j}, φ_{21}, φ_{22},…φ_{ij}]. As to the exponential functions, the *x*-axis and *y*-axis are arranged following their function wavelength, defined as:

$$\lambda_c = \frac{2\pi}{\sqrt{\left(\frac{2i\pi x}{L_x}\right)^2 + \left(\frac{2j\pi y}{L_y}\right)^2}}. \tag{21}$$

It can be observed in Fig. 7a that the condensed impedance terms of the exponential functions are much larger on the diagonal area than that on the off-diagonal area. This phenomenon indicates that the condensed impedance terms of exponential functions are strongly coupled only with themselves and their conjugate functions. Other combinations (in the non-diagonal area) generate small values so that they can be removed in the calculations, which leave rooms for reducing the computation cost and getting approximations with CTF method. For the $Z^a_{kl,ij}$ of the gate functions in Fig. 7b, it can be seen that the condensed impedance are not as concentrated as that of the exponential functions. As a result, the impedance matrix will not be diagonally dominated. All combinations of *ij* and *kl* are of importance during the calculation, showing the difficulty in reducing the matrix size using gate functions.

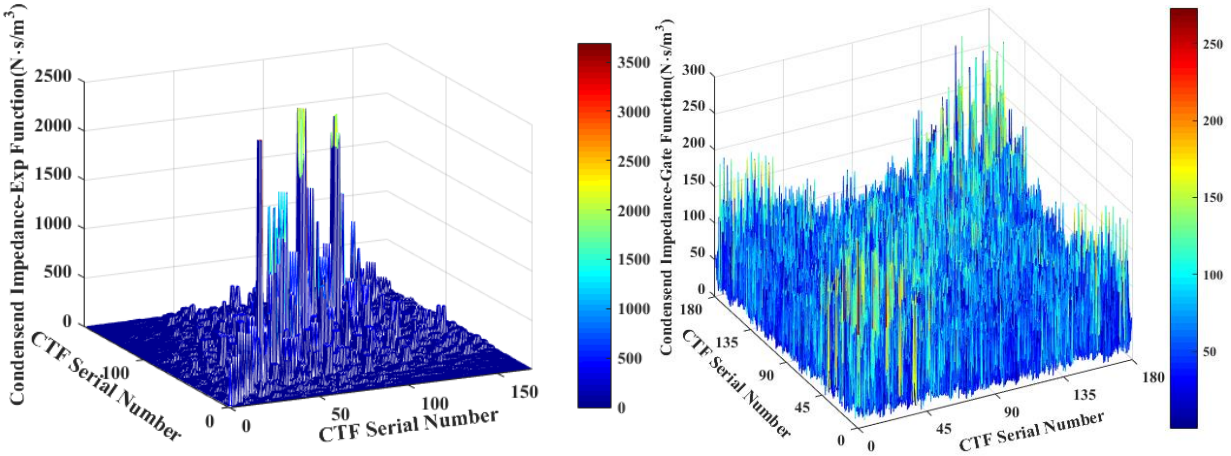

(a) (b)

Fig. 7 Condensed impedance of different condensation functions at 794 Hz: (a) exponential functions. (b) gate functions.

Similarly, the condensed mobility $Y^s_{kl,ij}$ for the vibrating plate is analyzed. The condensed mobility is calculated using the exponential functions and the gate functions, respectively. The frequencies of interest and the coordinate arrangements are the same as in Fig. 7. Again, one observes in Fig. 8a that the condensed mobility of exponential functions shows the dominance of the diagonal terms, as opposed to the case of the gate functions shown in Fig. 8b, in agreement with the observations made in Fig. 7b.

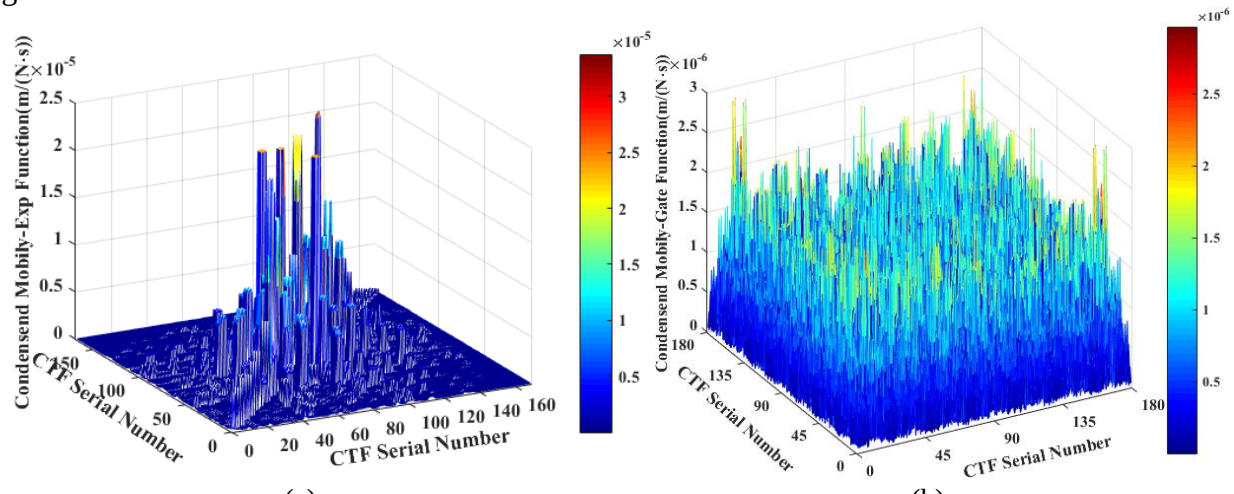

(a) (b)

Fig. 8 Condensed mobility of different condensation functions at 794 Hz: (a) exponential functions. (b) gate functions.

3.2.2 Condensed velocity

It is shown in the last subsection that the two uncoupled subsystems can be modelled more efficiently when the exponential functions are used instead of the gate functions. Whether the efficiency still maintains in the coupled system will be investigated in this subsection. Note that the coupling velocity is approximated in the CTF approach by Eq. (3).

Figure 9 shows the amplitude of $10log_{10}|u_{ij}|^2$, which represent the contribution of each condensation function φ_{ij} in the total system response, within the whole frequency band of interest. The *x*-axis denotes the frequency and the *y*-axis is the CTF serial number ij which is arranged in the same way as in Figs. 7 and 8. Figure 9a presents the velocity contribution u_{ij} when exponential functions are used. It can be seen that for each frequency, there are some terms holding a higher weight than the others and these high weighted terms change as the frequency increases, consistent with the analyses on the condensed impedance and condensed mobility. As to the gate function results shown in Fig. 9b, the contributions from different function terms are spread out, basically at any frequency within the frequency band of interest.

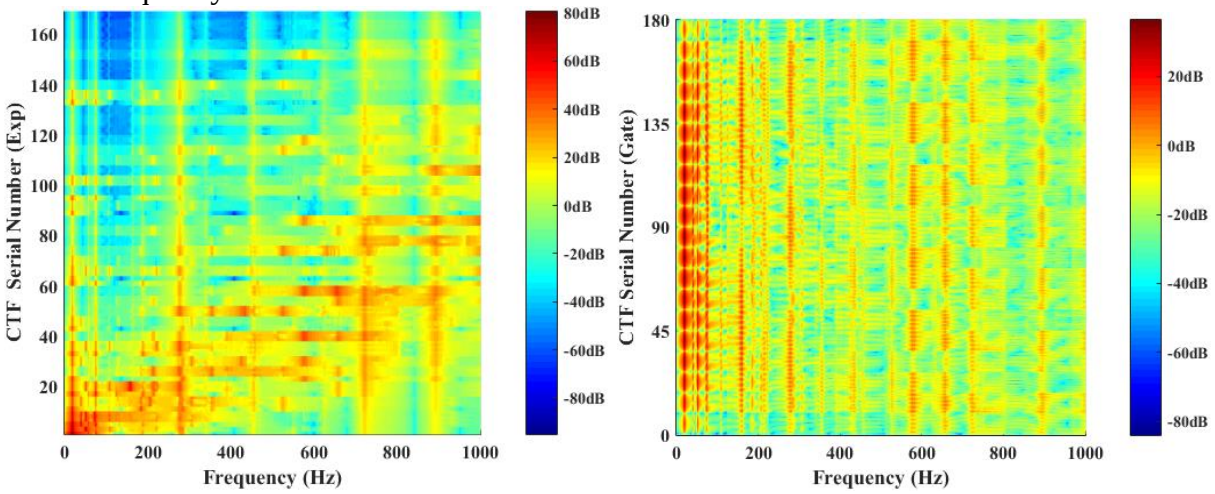

(a) (b)

Fig. 9 Condensed velocity of different condensation functions with respect to frequencies: (a) exponential functions. (b) gate functions.

The above analyses show the coupling and energy distribution feature of the exponential functions as compared with their gate functions counterparts. Results show a better prediction accuracy of the former and a confined coupling and energy distribution pattern across different CF terms.

4. Conclusions

Aiming at the modelling of the coupled vibro-acoustic system at mid-to-high frequency range, the condensed transfer function method has been re-examined. The method uses an orthonormal set functions to describe the force and velocity on the coupling surface of each subsystem, before being coupled together through the force equilibrium and velocity continuity. The condensation functions can be any functions satisfying the orthogonal condition. When the gate functions are used, the CTF method retreats to the previously proposed PTF method. In this paper, the CTF method is applied to modelling a panel-cavity system as a benchmark example. The validity of the CTF method is verified through comparisons with the reference solution, for both gate functions and exponential functions. It is found that the exponential function can model the coupled system more efficiently with a better accuracy than the gate functions. Meanwhile, a confined coupling and energy distribution pattern across different exponential CF terms are observed. It can then be surmised that this could be due to the wavy character of the functions and their spatial matching with the acoustic or structural waves involved. This points at the possibility of using less exponential functions terms to achieve the desired calculation accuracy in a prescribed frequency band. This point will be scrutinized in our future work.

REFERENCES

1 M. Ouisse, L. Maxit, C. Cacciolati and J. Guyader, "Patch transfer functions as a tool to couple linear acoustic problems," *Journal of Vibration and Acoustics* **127**(5), 458-466 (2005).

2 L. Maxit, M. Aucejo, and J.L. Guyader, "Improving the patch transfer function approach for fluid-structure modelling in heavy fluid," *Journal of Vibration and Acoustics* **134**(5), 051011 (2012).

3 L. Maxit, C. Cacciolati, and J. Guyader, "Airborne noise prediction using patch acoustic impedance," *Proceedings of ICSV* **9** (2002).

4 J. D. Chazot and J. Guyader, "Prediction of transmission loss of double panels with a patch-mobility method," *The Journal of the Acoustical Society of America* **121**(1), 267-278 (2007).

5 X. Yu, L. Cheng, and X. You, "Hybrid silencers with micro-perforated panels and internal partitions," *The Journal of the Acoustical Society of America* **137**(2), 951-62 (2015).

6 V. Meyer, L. Maxit, J. Guyader, T. Leissing, and C. Audoly, "A condensed transfer function method as a tool for solving vibroacoustic problems," *Proceedings of the Institution of Mechanical Engineers, Part C: Journal of Mechanical Engineering Science* **230**(6), 928-938 (2015).

7 V. Meyer, L. Maxita, J. Guyader, and T. Leissing, "Prediction of the vibroacoustic behavior of a submerged shell with non-axisymmetric internal substructures by a condensed transfer function method," *Journal of Sound and Vibration* **360** 260-276 (2016).